



Gold nanoparticles in cardiovascular imaging

Mariana Varna,^{1,2*} Hoa V. Xuan^{1,3} and Emmanuel Fort¹

Although originally applied in the field of oncology, recent results have illustrated the considerable potential of gold nanoparticles (GNPs) in the imaging of cardiovascular diseases (CVDs). CVDs represent the leading cause of mortality and disability in the world. The principal cause underpinning CVDs is atherosclerosis, which develops into mid and large blood vessels, often leading to severe complications. Thanks to their unique physicochemical properties, GNPs have drawn much attention from the research community in cardiovascular imaging. Thus, the optical properties of GNPs have led to their utilization as contrast agents for optical or X-ray imaging modalities allowing the detection of atherosclerotic plaques, intravascular thrombus, or fibrotic tissue. In this study, we detail the most promising preclinical scientific progresses based on the use of GNPs for imaging in cardiovascular field and their improvements for a potential clinical application. © 2017 Wiley Periodicals, Inc.

How to cite this article:

WIREs Nanomed Nanobiotechnol 2017, e1470. doi: 10.1002/wnan.1470

INTRODUCTION

The use of gold for therapeutic purposes dates back to antiquity in China and Egypt.¹ Nevertheless, only in recent decades the scientific community has shown a particular interest for applications of gold at nanometric size in the medical field, not only for therapeutic, but also for medical imaging application as contrast agents. The strong interest for biomedical utilization of gold nanoparticles (GNPs) relies on multiple characteristics. First, GNPs can easily be synthesized by using a variety of strategies including chemical, thermal, electrochemical, and sonochemical methods.² This enabled the development of GNPs with various shapes (e.g., spheres, rods, cages, prisms, stars, and crescents)^{3,4} and with sizes between 1 and 500 nm.^{1,5} Secondly, GNPs are inert, biocompatible, and can be

easily modified for targeting.^{6,7} The GNPs can react with molecules containing soft functional groups such as thiols or amines⁸ allowing for their biofunctionalization with different ligands (peptides, proteins, and aptamers)⁹ for specific recognition of biological targets. Different data showed that the hydrodynamic diameter, shape, and the biofunctionalization can affect the half-life into the body. The diameter of GNPs is inversely proportional to the speed of glomerular filtration.¹⁰ To avoid the rapid elimination of GNPs by the body, a common strategy is based to the use of polyethylene glycol (PEG). This increases the hydrophilicity of GNPs and improves the circulation time into the body by limiting the opsonins recognition.

Mainly developed for cancer imaging, the applications of GNPs in cardiovascular field is still in its infancy. In the following, we present a detailed overview of preclinical imaging with GNPs in the cardiovascular field. We first describe the unique optical and chemical properties of GNPs, which make them promising probes for bioimaging and cardiovascular therapies. After a short description of atherosclerotic plaque, the main underpinning of cardiovascular diseases (CVDs), the review examines how GNPs can improve optical or X-ray imaging, in order to evaluate plaque development or to detect an intravascular thrombus and the cardiac fibrosis.

*Correspondence to: mariana.varna-pannerec@u-psud.fr

¹Institut Langevin, ESPCI Paris, CNRS, PSL Research University, Paris, France

²Institut Galien Paris-Sud UMR 8612, CNRS, Université Paris-Sud/Paris-Saclay Faculté de Pharmacie, Châtenay-Malabry, France

³Faculty of Physics and Technology, Thai Nguyen University of Science (TNUS), Thai Nguyen, Vietnam

Conflict of interest: The authors have declared no conflicts of interest for this article.

PLASMONIC PROPERTIES OF GNPs

GNPs possess unique optical properties: the interaction between the free electrons of the GNPs with light induces their collective oscillations in resonance with the frequency of the absorbed light.¹¹ This phenomenon, called localized surface plasmon resonance (LSPR) (Figure 1), results in strong light absorption and scattering. This resonance can be tuned in a precise manner by changing the shape or size of the nanoparticles throughout the entire visible and near infrared (NIR) spectrum. The enhanced interaction between light and the particle at the LSPR give rise to both absorption (i.e., heat conversion) and scattering, which can also be tuned by varying the nanoparticle size and shape. For example, GNPs with a diameter smaller than 20 nm essentially absorb light, while GNPs with a diameter of 80 nm induce a strong scattering. The scattering and absorption cross sections can be much larger than the geometrical cross section at the LSPR. A large scattering cross section is required for biological imaging based on light scattering.^{1,12} The advantage of tuning the LSPR in the NIR range, commonly called the 'therapeutic window,' is that it allows a deep light penetration into the biological tissues, low auto-fluorescence, and reduced light absorption.¹³

Three different GNPs classes are largely applied for *in vivo* imaging purposes. As shown by Jain and coworkers,¹² all of these types have optical cross-section a few orders of magnitude higher than conventional dyes. Nanospheres with a spherical dielectric core and a thin gold shell have resonance wavelength in the visible and IR range; nonetheless the tunability of the wavelength with size is limited. For nanoshells and nanorods, the resonance wavelength can easily be changed by modifying the ratio between the dielectric core and gold shell or the rod aspect ratio, respectively.

Because of their unique optical and chemical properties, GNPs are attractive probes and can be used as contrast agents for different optical imaging

modalities including photoacoustic imaging (PAI), optical coherence tomography (OCT), and surface enhanced Raman scattering (SERS). These imaging modalities do not use harmful ionizing radiations.

Other non-optical imaging can use GNPs as contrast agents. Because of their physical properties, GNPs have been preclinically evaluated for X-ray imaging (computed tomography, CT). X-ray imaging is one of the most common imaging techniques in clinical practice thanks to its good spatial resolution (50–200 μm).^{14,15}

DEVELOPMENT OF THE ATHEROSCLEROTIC PLAQUE

CVDs (Box 1) are the leading cause of death and disability in the world.^{16,17} Coronary artery disease (CAD), stroke, and peripheral artery disease, all involve atherosclerosis. Atherosclerosis is a multifactorial and slowly progressing pathophysiological disease, which develops in large and mid-sized arteries at predisposed regions (e.g., near branch points and along inner curvature) characterized by disturbed blood flow dynamics.^{18–21} The development of atherosclerosis is linked to some risk factors such as hypertension, smoking, diabetes, high total cholesterol, excessive food intake, and physical inactivity or genetic hyperlipidemia.¹⁷ Atherosclerosis is initiated by structural and endothelial cell dysfunction in the arterial wall, and is characterized by a chronic inflammatory process.^{22,23} In this favorable inflammatory condition, low-density lipoproteins (LDLs)-derived cholesterol, extravasate through the defective endothelium into the subendothelial space (Figure 2). Thereafter, the lipoproteins undergo modifications by radical oxygen species and other enzymes such as myeloperoxidase, 15-lipoxygenase leading to the formation of oxidized LDL (oxLDLs).

The oxLDLs induce an inflammatory process manifested by the recruitment of monocytes and their attachment to the activated endothelial cells expressing adhesion molecules [e.g., selectins, vascular cell adhesion molecule 1 (VCAM-1), and intercellular adhesion molecule-1 (ICAM-1)]. The monocytes penetrate into subendothelial space and are subsequently differentiated into macrophages expressing scavenger receptors (SR-A/B and CD36). These macrophages will recognize the oxLDLs and will start to ingest them. When the uptake exceeds the efflux, lipids accumulate into macrophages, which become "foam cells." In the advanced atherosclerotic plaque, the pro-inflammatory cytokines (such as tumor necrosis factor- α and interleukin-6) will promote smooth

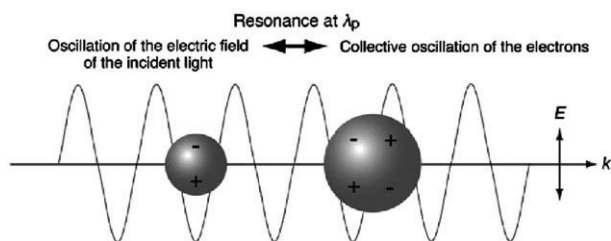


FIGURE 1 | Schematic diagram illustrating a localized surface plasmon. (Reprinted with permission from Ref 11. Copyright 2011 Royal Society of Chemistry)

BOX 1

CARDIOVASCULAR DISEASES

CVDs are a group of disorders among which are included:

Coronary heart diseases occur when the coronary blood flow is blocked by a blood clot or an atherosclerotic plaque. When the blockage is partial it can cause angina (chest pain) and when the blockage is complete, it can cause a myocardial infarction. The reestablishment of blood flow (reperfusion) may induce new cellular and tissue lesions known as ischemia/reperfusion lesions.

Stroke (ischemic or hemorrhagic) appears when a blood vessel that feeds into the brain is blocked, leading to a lack of blood and oxygen to the brain.

Peripheral arterial diseases occur when blood vessels supplying the arms and legs are blocked by an atherosclerotic plaque or by a clot.

Aortic aneurysms represent the second most frequent disease of the aorta after atherosclerosis. An aneurysm is generally defined as arterial enlargement with loss of arterial wall parallelism. Depending on the localization, there are thoracic aortic aneurysms (TAA) and abdominal aortic aneurysms (AAA).³⁰

Deep vein thrombosis and pulmonary embolisms are defined by the formation of a blood clot in the deep leg vein; the thrombus can break, travel in the circulation system, and become trapped in the lung inducing a pulmonary embolism.

muscle cells (SMCs) proliferation, gain macrophagic capacities, and can uptake oxLDLs contributing to foam cell formation. In parallel, SMCs participate in the fibrous cap development.^{18,24–26} During the development of atherosclerotic plaque, endothelial cells, macrophages, and SMCs die contributing to necrotic core formation within the plaque.^{27,28} This inflammatory environment promotes the development of fragile and defective blood vessels, mainly originating from *vasa vasorum*, and provides an alternative entry pathway for monocytes and immune cells. These neovessels tend to be fragile and prone to leakage, promoting intraplaque hemorrhage, and thus accelerating plaque growth and instability.²³ Another phenomenon observed during progressive atherosclerotic lesions is represented by

the presence of calcium microscopic granules deposits into the necrotic core.²¹

Plaque rupture can occur where the fibrous cap is thinner and is favored by proteolytic enzymes such as matrix metalloproteinase.²⁰ The contact between the necrotic core and the blood leads to a luminal thrombosis. The thrombus development is initiated by tissue factor, and culminates with the recruitment and generation of thrombin and fibrin.²⁹ The complications induced by thrombosis (e.g., myocardial infarction and stroke) are the most common causes of death and disabilities, while the atherosclerosis alone is rarely fatal. Identification and localization of vulnerable plaques (e.g., macrophages accumulation, intraplaque hemorrhages, or thin fibrous cap) are therefore essential to avoid the complications because of their rupture.

According to Mathers and Loncar,³¹ by 2030, over 23.3 million people will die annually from CVD. Increased knowledge of the atherosclerotic mechanism as well as the complications induced by the thrombus formation had led to the identification of molecular markers, which are ideal targets for imaging and therapy. Nowadays, there is a strong need to improve the sensitivity of the current imaging modalities in atherosclerosis and, overall, on CVDs. Different imaging modalities are developed and used in clinical practice for diagnosis and follow-up of the CVDs (Box 2). However, these imaging methodologies also show some limitations. Thus, early detection, the precise follow-up of these diseases and the prediction of acute clinical events caused by atherosclerotic plaque rupture remain a major clinical challenge.

In the next section, we highlight the relevance of GNPs as contrast agents for optical imaging modalities in preclinical development and their applications for X-ray imaging.

GNPs IN CARDIOVASCULAR OPTICAL IMAGING

Photoacoustic Imaging

The photoacoustic effect was discovered by Alexander Bell over 100 years ago. The absorption of optical or radiofrequency waves leads to local heating and thermoelastic expansion which can generate transient acoustic signal.^{13,47} PAI is a hybrid experimental imaging modality that combines the optical and ultrasound imaging techniques. It provides information with a high spatial resolution (50–500 μm) and penetration depth up to 5 cm.⁴⁸ This imaging modality is based on the photoacoustic effect and is

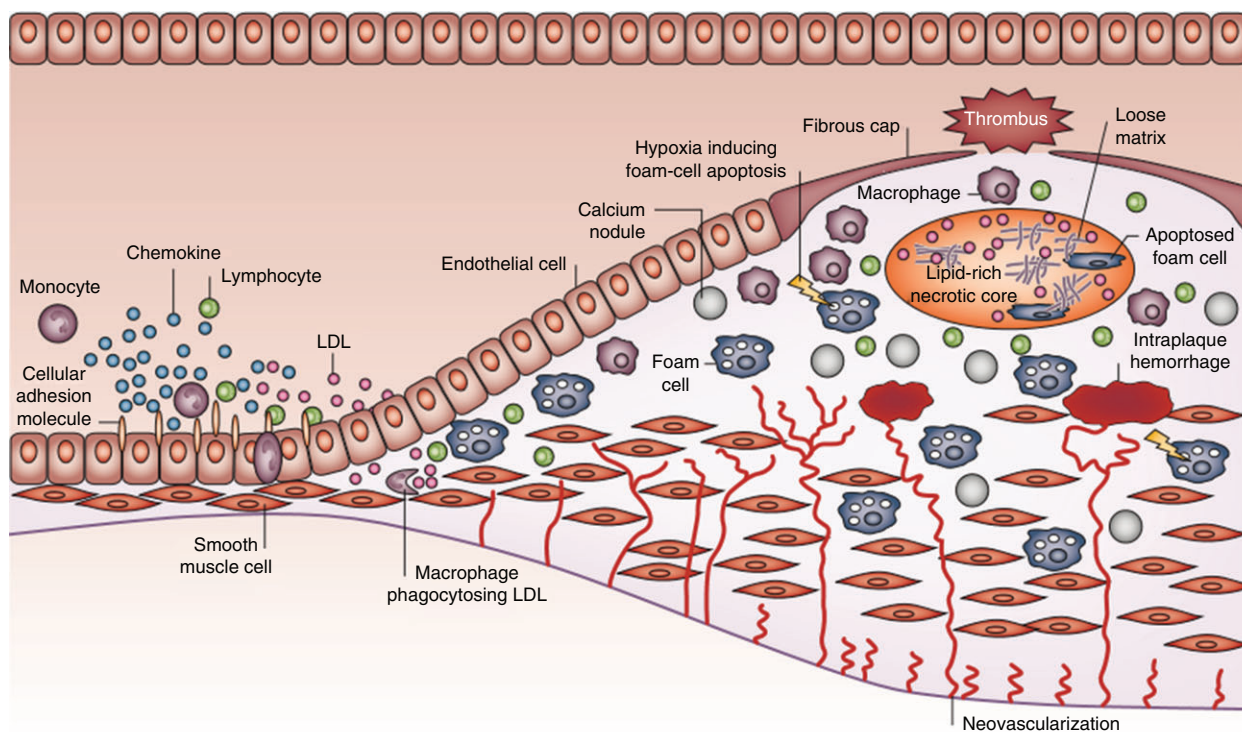


FIGURE 2 | The main steps in atherosclerotic plaque development. The risk factors (e.g., hypertension and dyslipidemia) lead to activation of endothelial cells that start to express adhesion molecules. The monocytes can then adhere to the endothelium and accumulate into the subendothelial space; here they are transformed into macrophages and start to ingest oxidized low-density lipoprotein (oxLDL) and become foam cells. In this inflammatory environment, the smooth muscle cells (SMCs) migrate, proliferate, and produce collagen. New fragile neovessels are formed and may bleed, causing intraplaque hemorrhages and participating in plaque growth. At the advanced stage of atherosclerosis, a fibrous cap is formed encapsulating a necrotic core with calcium microcrystals. (Reprinted with permission from Ref 23. Copyright 2015 Macmillan Publishers Ltd)

related to the optical properties of different tissues. PAI offers the possibility of imaging both intrinsic tissue molecules (e.g., hemoglobin, lipids, water, and melanin) and exogenous contrast agents like GNPs. PAI uses pulsed laser beams, usually at nanosecond range. These short pulses of light are absorbed in tissues inducing a localized thermoelastic expansion, which generates acoustic waves detectable by an ultrasound transducer.^{49,50}

Two configurations of PAI have been proposed: photoacoustic tomography (PAT), used at centimeter imaging depths, and photoacoustic microscopy, used at millimeter imaging depths. Briefly, PAT uses a short-pulse laser beam to induce thermoelastic expansion of absorbers, which then produces pressure acoustic waves (Figure 3). The waves are detected by a wideband ultrasonic transducer and are used to reconstruct the three-dimensional (3D) tissue absorption distribution.⁵¹

Exogenous contrast agents are employed for better tissue detection. For example, one of the most commonly used contrast agents is Indocyanine green (ICG), an Food and Drug Administration-approved

dye. ICG shows a high molecular extinction coefficient with high photoabsorbance, but poor stability and rapid excretion.^{52–54} Thus, to visualize the vasculature, multiple ICG dyes injections are needed.⁵⁵ Other molecules are also used, such as methylene blue (664 nm) and Evans blue (620 nm), which are limited by their blue-shifted absorption peaks and photodamage under strong radiation.^{56–58}

To overcome the limitations of classical dyes, GNPs with different shapes have been tested as contrast enhancement agents (Table 1).^{61,71–74} For example, poly-ethylene glycol (PEG)-coated hollow gold nanospheres have been successfully applied to visualize the brain vasculature in living mice (Figure 4(a)). These NPs composed of a thin gold wall display a strong absorption peak at 800 nm. The images depicted brain blood vessels as small as approximately 100 μm in diameter.⁵⁹ It should be noted that the PEG coating of GNPs is one of the most common strategies used to prolong circulation time into the body.

Rouleau et al.⁶⁰ have developed PEGylated gold nanoshells targeting VCAM-1, a known marker

BOX 2

CARDIOVASCULAR IMAGING

In this box are described some imaging modalities used in clinical practice:

Magnetic resonance imaging (MRI) signal originates from hydrogen atoms through magnetization and resonance after application of a radiofrequency pulse. The contrast can be enhanced by using gadolinium or fluorine-19 (^{19}F) as contrast agents. This noninvasive imaging technique can provide insights into the biological characteristics of the tissue of interest such as water, lipid, and fibrous cap content.³² When gadolinium is used as contrast agent, MRI can provide information on fibrous cap and necrotic core,³³ macrophage content, degree of plaque neovascularization,³⁴ intraplaque hemorrhage, and mural thrombus.^{34–36} MRI presents some disadvantages such as the cost of the setup and the impossibility of being conducted on some patients (with a pacemaker or claustrophobic patients). This imaging method is several magnitudes less sensitive than radionuclide and optical techniques.^{15,37} Another limitation could be linked to the use of gadolinium which can induce a small risk of nephrogenic systemic sclerosis, related to renal function in patients with end stage renal diseases on dialysis.

Positron emission tomography (PET) uses small amounts of radioactive materials called radiotracers. The most common used radiotracers in cardiovascular diagnosis are fluorine-18 (^{18}F) and gallium-68 (^{68}Ga). The glucose analogue 18F-fluorodeoxyglucose (^{18}F -FDG), which is taken up with high affinity by hypermetabolic cells (e.g., inflammatory cells) imaging has been set up in humans for imaging high-risk plaques. PET is often combined with CT imaging, which provides excellent anatomic information, allowing the identification of the culprit stenosis in patients presenting chest pain. PET/CT is a powerful noninvasive modality that offers the potential for refined diagnosis and management of coronary atherosclerosis.³⁸

Single-photon emission CT (SPECT) is another nuclear imaging modality used in the diagnosis or to assess the prognosis of CAD and heart muscle damage following an infarction. SPECT is based on the selective uptake of a radioactive tracer, thallium-201 (^{201}Tl), or technetium-99m ($^{99\text{m}}\text{Tc}$), by functional myocardial tissue. This method was developed to evaluate myocardial

perfusion and viability and is applied at rest and after exercise or pharmacological stress.³⁹

Echocardiography is a routinely imaging technique used in the diagnosis and follow-up of patients with suspected or known heart disease. It has been used essentially to provide mechanistic insights on cardiac morphology such as left ventricle mass or the estimation of the heart function. In echocardiography, the high-frequency ultrasound is directed into the body and then reflected by interfaces between tissues of different acoustic impedance such as myocardium, valves, and blood.³⁹ In order to diagnose CAD and assess a possible myocardial ischemia, an echocardiography after stress (induced by physical exercise or pharmacological agents) is one of the most commonly used imaging techniques in clinics. This rapid examination is very useful to assess risk stratification in patients with established CAD, to evaluate the severity of heart valve stenosis, to evaluate patients after revascularization, or to determine response to therapy and predict patient outcome.⁴⁰

Coronary angiography is one of the most applied imaging techniques for cardiovascular diagnosis or therapy guidance. This imaging method enables to obtain rapid anatomic two-dimensional (2D) imaging of blood vessels, with high spatial resolution. Some disadvantages of this imaging method are linked to the low sensitivity, the exposure to radiations, and the allergies developed to iodinated contrast agents.

A major limitation of coronary angiography is its insensitivity in detecting subclinical atherosclerosis and quantifying plaque burden because of remodeling of the atherosclerotic vessel.⁴¹

Intravascular ultrasound (IVUS) is a valuable diagnostic imaging technique which complete angiography. The principle is based on the use of a catheter with a tiny ultrasound band. The catheter inserted into an artery provides precise tomographic measurements of lumen area, plaque size, and to some extent the composition of atherosclerotic plaque. This imaging method is commonly used during angioplasty.⁴²

Optical Coherence Tomography (OCT) is a powerful optical imaging technique with axial sectioning based on light interference. OCT can be performed *in situ* and in real-time and provides 3D imaging.⁴³ The high resolution of OCT enables imaging of plaque architecture. OCT makes the visualization of surface

structure and composition of atherosclerotic plaque possible.⁴⁴ The major limitations of OCT are the requirement for a blood-free field to avoid light scattering by red blood cells, its invasiveness, and the poor penetration of light through lipid-rich tissues.^{45,46}

of early endothelial cell activation. After intravenous injection into ApoE-deficient mice (ApoE^{-/-}), the PAI allowed the detection of the atherosclerotic plaque, because the targeted nanoshells accumulated onto the plaque (Figure 4(b)). It is known that VCAM-1 is expressed on endothelial cells in both early and advanced atherosclerotic lesions as well as on activated macrophages and SMCs.⁷⁵ This could limit the translation on clinical imaging to detect vulnerable plaques by using this vascular marker.

Another kind of nanoparticle platform tested for PAI is represented by gold nanobeacons. With the aim to target the intravascular thrombus, Lanza's team developed gold nanobeacons targeting fibrin, as it is a critical component of the thrombus. They demonstrated in a rat model that the targeted nanobeacons provide a more than 10-fold signal enhancement in PAI when excited in the NIR spectral window.⁵¹ Later, the same team developed gold nanobeacons targeting $\alpha_5\beta_3$ -integrin, a heterodimeric transmembrane glycoprotein presented on the luminal zone of proliferating endothelial cells and considered as a neovascular biomarker. The authors

demonstrated that $\alpha_5\beta_3$ -integrin coated GNPs provided an efficient and sensitive means of detecting angiogenesis in a Matrigel-plug mouse model. This strategy offers the possibility to detect and quantify developing angiogenic bridges and sprouts undetectable in the baseline images.⁵¹ These results were explained by the specific accumulation of the targeted nanoparticles either into the thrombus or the endothelial cells. Because gold nanobeacons entrap multiple copies of tiny GNPs (2–4 nm), their mutual interaction can greatly amplify the signal and provide strong acoustic signal for PAI.

In addition, several other preclinical imaging applications of GNPs have been tested in the cardiovascular field. PAI using gold nanorods as contrast agents, coupled with focused-ultrasound, was performed to induce blood–brain barrier opening in a rat model.⁷⁶ This strategy allowed the monitoring of *in vivo* focused ultrasound effect. Other *in vitro* experiments have demonstrated the possibility of tracking stem cells⁷⁷ or macrophages⁷⁸ by using PAI. Loading GNPs into endosomal compartments of stem cells does not alter cellular functions including cell viability and differentiation.⁷⁷

Another elaborate strategy has been developed by the Emelianov team. This method, which combines intravascular ultrasound and intravascular photoacoustic (IVUS/IVPA) imaging, represents an attractive modality to assess atherosclerotic plaque and to detect lipid regions in the aorta.⁷⁹ IVUS provides morphological information but lacks sensitivity in the identification of lipid-rich plaques,⁸⁰ while IVPA enables imaging of the full arterial thickness. By using IVUS/IVPA (Figure 4(c)), the authors showed that gold nanorods colocalize with atherosclerotic regions after injection in rabbits with atherosclerotic plaques. *Ex vivo* results demonstrated a high photoacoustic signal from localized GNPs in regions with atherosclerotic plaques. These findings, confirmed on histological sections, were explained by the fact that the GNPs extravasate in atherosclerotic regions with compromised luminal endothelium and acute inflammation.⁶³ In another experiment, Emelianov and coworkers demonstrated that GNPs can aggregate after their uptake by the macrophages, one of the key components involved in the pathology of atherosclerosis. In addition, in a rabbit injected with macrophages loaded with GNPs, the authors were able to detect *ex vivo*, a strong photoacoustic signal in the area of rabbit aorta.^{62,81}

More recently, multispectral optoacoustic tomography (MSOT) offered the ability to visualize tissues based on their distinct spectral signatures after multiple illumination wavelengths.^{82–84} This method

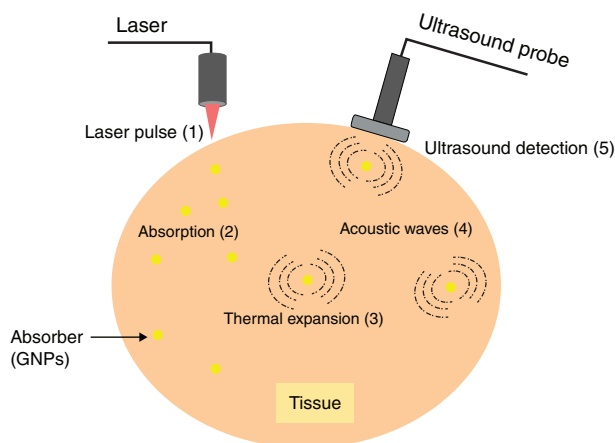


FIGURE 3 | Principle of photoacoustic imaging. Near infrared (NIR) laser (1) is applied on tissue containing gold nanoparticles (GNPs) (2), generating ultrasound waves (3, 4), detected by ultrasonic transducers (5).

TABLE 1 | Strategies in Preclinical Cardiovascular Imaging Using GNPs as Contrast Agents

Imaging Modality	NPs Shape	Size	Targeting Strategy	Animal Model	Detection	Way of Injection	Main Results	Ref
PAI	Nanospheres	~40 nm	No	Mouse	Brain vasculature	iv	2 h after iv injection, the images depicted brain blood vessel as small as ~100 μ m	⁵⁹
PAI	Nanoshells	~37 nm	VCAM-1	Mouse	Atherosclerotic plaques	iv	Targeting aortic arch Enhanced contrast for atherosclerotic plaque imaging	⁶⁰
PAT	Nanobeacons	~154 nm	No	Rat	Thrombus	iv	Gold nanobeacons provide more than 10-fold signal enhancement in PAT	⁶¹
PAI	Nanobeacons	~159 nm	$\alpha_v\beta_3$	Mouse	Angiogenesis in Matrigel-plug	iv	Integrin- $\alpha_v\beta_3$ targeted nanobeacons penetrated deep into the Matrigel-plug and bound the neovessels	⁵¹
IVPA/IVUS	Nanospheres	~50 nm	No	Rabbit	Atherosclerotic plaques	<i>Ex vivo</i> , in the outer and inner regions of the aorta	Detection of macrophages in atherosclerotic plaque due to a strong PA signal	⁶²
IVPA/IVUS	Nanorods	Less than 50 nm	No	Rabbit	Atherosclerotic plaques	iv	<i>Ex vivo</i> imaging reveal a high PA signal in atherosclerotic plaques	⁶³
PT-OCT	Nanoroses	~30 nm	No	Rabbit	Atherosclerotic plaques	iv	Estimation of the NPs concentration on excised aorta	⁶⁴
OCT	Nanoroses	~30 nm	No	Rabbit	Aorta inflammation	iv	Nanorose-loaded macrophages are <i>ex vivo</i> detected superficially within 20 μ m from the luminal surface	⁴⁴
SERS	Nanospheres	~100 nm	ICAM-1	Mouse	Early stages inflammation of atherosclerotic lesions	iv	SERS allowed noninvasive measurement of ICAM-1 expression <i>in vivo</i>	⁶⁵
Multispectral CT	Nanospheres	~7.2 nm	HDL	Mouse	Atherosclerotic plaques	iv	Accumulation of NPs-HDL were detected in the aorta of the mice	⁶⁶
CT	Nanospheres	~31 nm	No	Mouse	Atherosclerotic plaques	iv (NPs labeled monocytes)	Noninvasively <i>in vivo</i> tracking of labeled monocytes migration into atherosclerotic plaques	⁶⁷
CT	Nanospheres	~127 nm	No	Mouse	Thrombi in carotid arteries	iv	Direct thrombus imaging using GNPs	⁶⁸

(continued overleaf)

TABLE 1 | Continued

Imaging Modality	NPs Shape	Size	Targeting Strategy	Animal Model	Detection	Way of Injection	Main Results	Ref
CT	Nanospheres	~127 nm	Fibrin targeting peptide	Mouse	Cerebral thromboemboli	iv	Quantification and serial monitoring of thrombus lysis Fibrin-targeted GNPs allow the assessment of the location and thrombolysis of cerebral thrombi by using CT imaging	69
CT	Nanospheres	~50 nm	Collagen targeting peptide (CNA35)	Mouse	Myocardial scar	iv	Specific targeting of myocardial scar with the homing peptide Better tissue retention and enhanced X-ray attenuation	70

CT, computed tomography; GNPs, gold nanoparticles; HDL, high-density lipoprotein; ICAM-1, intercellular adhesion molecule-1; IVPA/IVUS, intravascular photoacoustic/intravascular ultrasound; OCT, optical coherence tomography; PAI, photoacoustic imaging; PAT, photoacoustic tomography; PT-OCT, photothermal-optical coherence tomography; SERS, surface-enhanced Raman scattering; VCAM-1, vascular cell adhesion molecule 1.

uses a nanosecond pulsed light from multiple wavelengths to illuminate the tissue to analyze. After the absorption of light pulses, the thermoelastic expansion of tissue generates ultrasound waves. The amplitude of the generated ultrasound waves depend on the local light fluence and optical absorption capacities of the biological tissues. By using MSOT imaging, Taruttis et al. were the first to image *ex vivo* gold nanorods into the carotid arteries, the aorta, and the heart.⁸⁵ Later, they applied this imaging strategy to visualize *in vivo* mouse heart⁸⁶ or myocardial infarction in a murine model of coronary artery ligation.⁸³

These preclinical results demonstrated that GNPs could be applied in PAI as well as on hybrid imaging methods (IVUS/IVPA) for CVDs assessment. By using PAI modalities, these different teams have demonstrated that the employment of GNPs is an attractive means to target and to visualize atherosclerotic plaque *in vivo* in small animals as well as *ex vivo*. However, fewer limitations may still be addressed for clinical implementation. These limitations are principally linked to the deep localization of the lesion in humans and the degree of sensibility of lesion detection by using GNPs.

Optical Coherence Tomography

OCT is an emerging noninvasive imaging modality, which provides images with axial and lateral resolution of 10 and 20–40 μm , respectively,⁴⁶ while the tissues depth penetration is up to 2 mm. The

principle of this technique (Figure 5) is based on the directing of a beam of NIR light from a broad-band coherent light source to a targeted biological tissue and capturing light that is backscattered from that tissue. Depth information is obtained from the detection of interferences between the backscattered light and the light reflected from a reference mirror.⁸⁷ The low-coherence length resulting from the broadband light source results in a precise axial sectioning.^{88,89} Contrast is obtained from the various scattering signatures of biological materials and architectures.

OCT was initially demonstrated in clinical practice for retinal imaging, which was followed by applications in new clinical areas such as dermatology or vascular diseases.^{90–92} OCT can assist in determination of diverse histological constituents of atherosclerotic plaque. As OCT imaging is sensitive to hemoglobin, the major absorber of the light in tissues, this imaging method was employed to visualize vascularization in clinical setting⁹³ and to determine the different histological constituents. OCT enables high-resolution characterization of vascular layers and can identify morphological changes of the atherosclerotic plaques including fibrous and calcified lesions.^{32,80,94,95}

The utility of OCT can be further enhanced by using external contrast agents. However, the traditional fluorescent and bioluminescent probes do not emit coherent light, and thus provide no contrast with OCT. Because GNPs exhibit large optical scattering or absorption cross sections, different reports have demonstrated that the GNPs can be used to provide contrast enhancement in OCT for *in vivo*

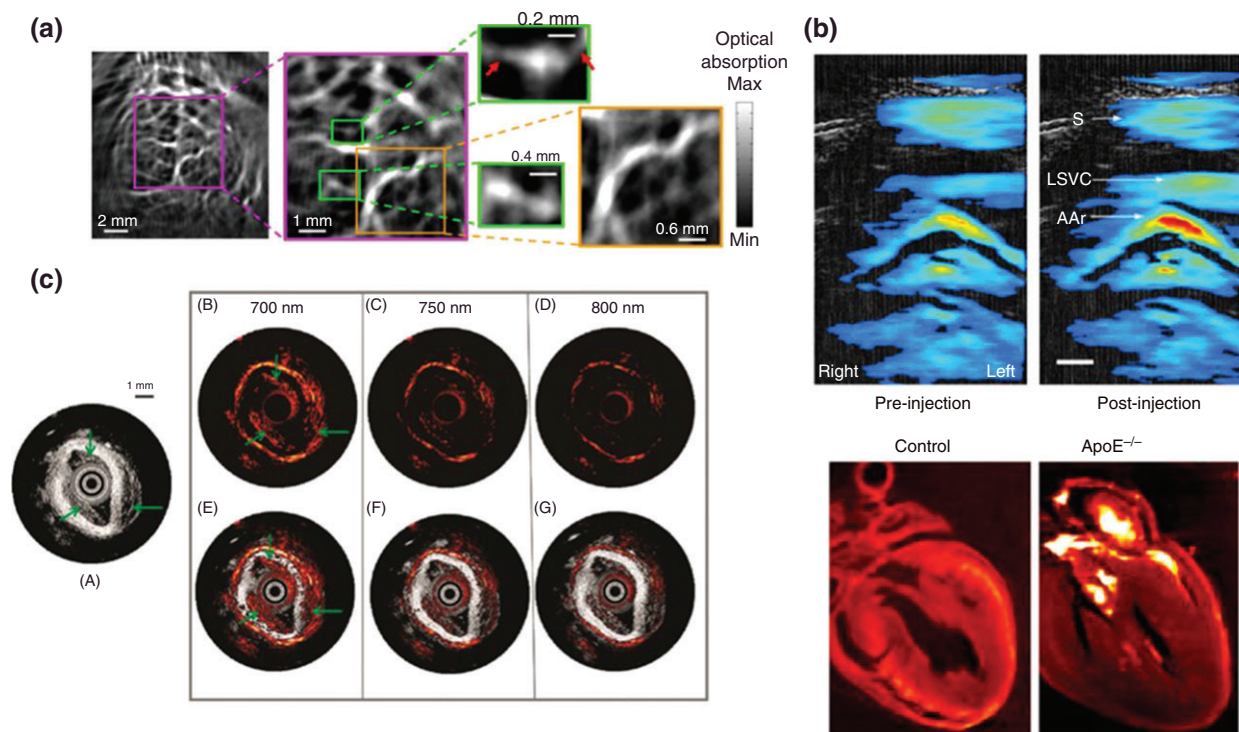


FIGURE 4 | Some examples of *in vivo* photoacoustic imaging application in the cardiovascular field using gold nanoparticles (GNPs) as contrast enhancement agents. (a) Enhanced photoacoustic (PA) signals revealed large (yellow-framed picture) and small (green-framed picture) blood vessels in mouse brain 2 h after intravascular (IV) injection of PEGylated GNPs. Small blood vessels with a diameter $\sim 100 \mu\text{m}$ are indicated by arrows. (Reprinted with permission from Ref 59. Copyright 2016 American Chemical Society). (b) Upper panel: View of parasternal short axis, aortic arch area in one animal pre- and postinjection ($t = 3 \text{ min } 20 \text{ s p.i.}$) (S, sternum; AAr, aortic arch; LSVC, left superior vena cava. Bar 1 mm). Bottom panel: Illustrative example of control results and $\text{ApoE}^{-/-}$ mice in optical projection tomography, with localization of vascular cell adhesion molecule 1 (VCAM-1)-targeted immunonanoshells in the aortic arch. (Reprinted with permission from Ref 60. Copyright 2012 John Wiley & Sons, Ltd). (c) Intravascular ultrasound (IVUS), intravascular photoacoustic (IVPA), and combined IVUS/IVPA images obtained on a section of aorta extracted from a rabbit with high cholesterol diet for 3 months. Macrophages loaded with GNPs were injected into the outer and inner boundary of the aorta. Area of injection is indicated with green arrows (A, B, E). The IVUS image (panel A) is displayed using 50 dB dynamic range. The normalized IVPA images (panels B–D) and combined IVUS/IVPA images (panels E–G) were taken using 700, 750, and 800 nm wavelength. High photoacoustic signal on the injected regions is obtained with the IVPA and combined IVUS/IVPA (panels B and E). (Reprinted with permission from Ref 62. Copyright 2009 American Chemical Society)

high-resolution imaging (Table 1).^{96–99} For example, gold nanoshells are attractive contrast agents for OCT because they resonate in the NIR, where OCT typically operates, and have a high backscattering coefficient.^{100,101} Zagaynova et al.¹⁰² demonstrated that the injection of nanoshells into rabbit skin increases the signal brightness in OCT and allows delimitation between the area with nanoshells and the area without nanoshells.

Photothermal OCT (PT-OCT) uses photothermal heating, where photon absorption by a target (e.g., GNP) leads to a temperature increase in the environment surrounding the target, causing thermoelastic expansion of the sample, shifts in the local index of refraction, and alteration of the local optical path length. Thus, PT-OCT provides molecular contrast by combining phase sensitive OCT with laser

excitation of targeted chromophores to measure optical path length variation.^{103–105} Using this imaging strategy, Paranjape et al.⁶⁴ detected the presence of macrophages loaded with gold nanoroses on *ex vivo* rabbit atherosclerotic arteries. The nanoroses engulfed by macrophages were injected into rabbits with atherosclerotic plaque into ear vein and analyzed 3 days later. This strategy allowed the estimation of nanorose concentration in atherosclerotic lesions as these regions were rich with macrophages loaded with nanoroses. Later, by using the same strategy, Wang et al.^{44,76} detected the presence of macrophages loaded with gold nanoroses as well as lipid deposits in atherosclerotic plaques (Figure 6). The authors concluded that the nanorose loaded macrophages could be detected superficially within $20 \mu\text{m}$ from the luminal surface of the aorta.⁴⁴

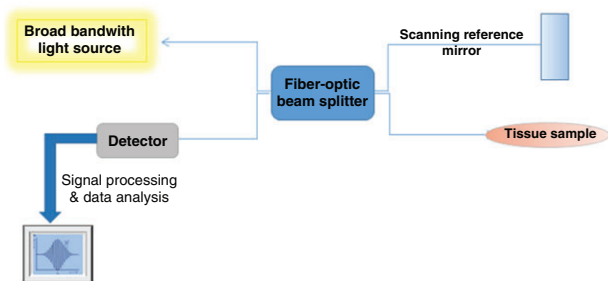


FIGURE 5 | Principle of optical coherence tomography (OCT). OCT is based on white-light interferometry, in which interference signals are only detected if the light in the sample and in the reference arm has traveled equal distances within the coherence length of the source.

Recently, in an experimental procedure, Hu et al.¹⁰⁶ have found that gold nanoshells provide the best contrast enhancement by using a clinical intracoronary 3D OCT catheter. The next step would be the validation of these results *in vivo* in a real pathophysiological condition.

These results demonstrate that OCT with plasmonic GNPs as contrast agents can offer new applications in cardiovascular molecular imaging opening the perspective to monitor based plaque macrophages loaded with GNPs overtime. A problem could arise for

clinical imaging application, which is linked to the fact that the biodistribution of GNPs into plaque could be nonuniform and thus induce false results.

Surface-Enhanced Raman Scattering

Raman spectroscopy is a spectroscopic nonlinear optical technique, which allows the molecular detection of biomolecules based on the inelastic scattering of light.¹⁰⁷ SERS has emerged as an alternative to fluorescence-based spectroscopy as it significantly increases the sensitivity of Raman spectroscopy and it enables label-free measurements. Advantages of SERS include the remarkable multiplexing capacity, the quantification of SERS signatures, and the high photostability.^{108,109} As SERS is a noninvasive and highly sensitive imaging modality, it has been used for visualizing and quantifying the distribution of target molecules such as proteins in cells and tissues,^{110–112} mainly for sentinel lymph node mapping and tumor targeting in mice.¹¹³

The Raman phenomenon was discovered in 1974 by Fleischmann and coworkers and has largely been used since in Raman spectroscopy.^{114,115} However, its very small molecular cross section has strongly limited its sensitivity. When molecules are adsorbed onto the metallic nanoparticles surface, they undergo a

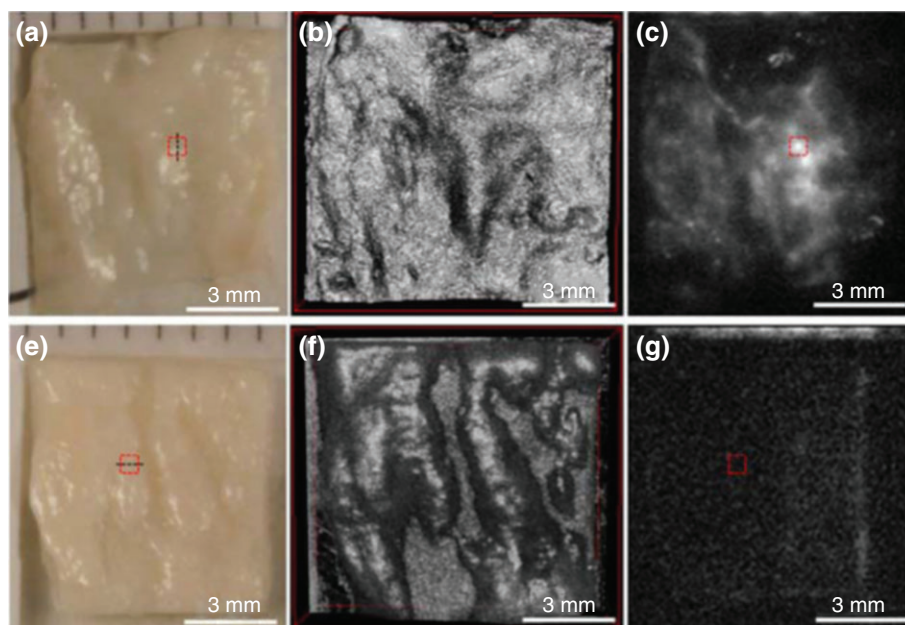


FIGURE 6 | Detection of gold nanoroses on abdominal aorta surface by using optical coherence tomography (OCT) in combination with two-photon luminescence (TPL) microscopy on aorta from rabbits. Images a–c are from Positive rabbit (with nanorose) and images e–g are from Control rabbit (with saline buffer). Images a and e show unstained histological sections of surface aorta. Images b and f show detailed surface structure of aorta segments with peak and valley regions, which are clearly visible in the three-dimensional (3D) OCT. Nanorose is also detected by TPL microscopy in the same aorta segment as denoted by the red boxes (c) but no signal in control mice (g). (Reprinted with permission from Ref 44. Copyright 2012 John Wiley & Sons, Ltd)

dramatic enhancement of the Raman signal because of the local strong electric field amplification resulting from the plasmonic resonance.^{4,116} Moreover, the optical interaction being nonlinear, sensitivity can reach that of single molecule detection.³ Various organic dyes, such as Cy3, Cy5, 3,3'-diethylthiatri-carbocyanine, and rhodamine, are used for Raman spectroscopy applications.^{4,109,117–119} For *in vivo* applications, gold provides an excellent choice because of its strong plasmonic resonance and its chemical stability as well as its biocompatibility.

In the cardiovascular field (Table 1), McQueenie et al.⁶⁵ have used SERS imaging for the first time to detect inflammation, one of the key mechanisms in the development of different stages of atherosclerosis. They used SERS-GNPs targeting ICAM-1, a protein expressed by endothelial cells principally during inflammation. Using SERS imaging (Figure 7), the authors were able to identify expression levels of ICAM-1 on *ex vivo* tissue sections of the ApoE-deficient mice. The authors concluded that this strategy could open the way for new applications in inflammation detection of rheumatoid arthritis or even parasitology.

Yet, the major limitation of SERS in CVDs is its limited deep detection in the body. For *in vivo* imaging applications, improvements of the devices as well as of the exogenous contrast agents are mandatory. Moreover, additional studies are required in order to investigate the *in vivo* toxicity of the Raman-GNPs over short and long-term periods of time.

CT Imaging

X-ray CT is a noninvasive diagnostic imaging technique in clinical practice. It allows fast 3D anatomic

imaging with a good spatial resolution (50–200 μm) and deep tissue penetration.^{14,120} X-ray imaging is based on the principle that a detector measures the attenuation of X-ray photons when they pass through the body.¹⁴ However, these systems require delivery of barium sulfate suspensions or iodinated contrast agents to better distinguish tissues with similar or low X-ray attenuation.^{121–123} These contrast agents show limitations linked to their *in vivo* short circulation time because of their rapid clearance by the kidney and thus a short imaging window. Hypersensitivity to iodine and potential damage to the kidney in some patients was equally noted.¹²⁴

GNPs have gained attention as an X-ray contrast agent following initial reports by Hainfeld et al. in 2004 and 2006.^{125,126} The use of GNPs for X-ray contrast-enhanced imaging is based on the fact that gold possesses a high atomic number ($Z_{\text{Au}} = 79$) and high mass absorption coefficient which provide 2.7-fold greater X-ray contrast per unit weight than iodine.^{14,123,126} Furthermore, the K-edge energy for gold (80.7 KeV) is higher than the K-edge for iodine-based contrast agents (33.2 KeV) suggesting that a better contrast would be achieved with gold. Moreover, absorption edge subtraction can be used to increase the signal-to-noise ratio by subtracting images taken at energy levels above and below the K-edge of GNPs.^{122,127} Thus, the unique properties of GNPs, including small size, biocompatibility, increased circulating half-life when PEGylated, targeting capacity, and high atomic number make them appealing as contrast agents for *in vivo* CT-imaging assessment. GNPs were evaluated in preclinical CVDs models (Table 1). By using GNPs targeted with a high-density lipoprotein (GNPs-HDL) and a multicolour (spectral) CT, Cormode et al.⁶⁶ have

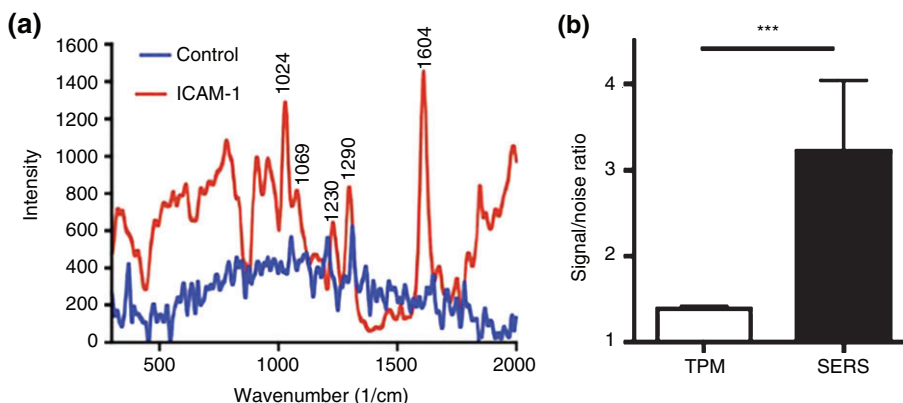


FIGURE 7 | Examples of surface enhanced Raman scattering (SERS) spectroscopy. (a) Mice receiving intravenous injections of anti-intercellular adhesion molecule-1 (anti-ICAM-1)-conjugated nanotags (red) but no apparent spectra in mice with intravascular (IV) injections of control (IgG2b) nanotags (blue). (b) Signal-to-noise ratio of ICAM-1/control shows greater signal-to-noise for SERS compared with Two-Photon fluorescence Microscopy (TPM). *** $P < 0.001$. (Reprinted with permission from Ref 65. Copyright 2012 American Chemical Society)

visualized *in vivo* accumulation of GNPs in macrophages rich plaques in ApoE^{-/-} mice. CT imaging methods that sample an entire X-ray spectrum with allocation of X-rays in multiple spectra are called spectral (multicolor) CT.¹²⁸ The CT imaging was used to track the recruitment of monocytes into atherosclerotic plaque. The recruitment of monocytes from circulation has been found to correlate with the progression and severity of atherosclerosis. Their accumulation and detection could thus be useful for identifying atherosclerotic plaque *in vivo*. In another approach, Chhour et al.⁶⁷ labeled primary monocytes with GNPs (15 nm in diameter) before injecting them into ApoE-deficient mice (Figure 8, left panel). By using a micro-CT scanner, they identified *in vivo* the monocytes loaded with GNPs inside the plaque. This strategy outlines new opportunities for *in vivo* identification and management of atherosclerotic plaque. Moreover, these results give a new perspective to a theranostic approach by simultaneously using GNPs as therapeutic platforms and imaging contrast agents. After further preclinical investigations, this strategy could be applied in clinics to detect the vulnerable plaque and thus the high-risk patients.

Later, Kim et al.⁶⁸ injected GNPs to visualize, using CT, the presence and the extent of thrombi in

mouse carotid arteries. They were able to detect the therapeutic efficacy of the thrombolysis with tissue plasminogen activator. More recently, the same team injected glycol/chitosan-coated GNPs conjugated with fibrin targeting peptides in mice with carotid thrombus and/or embolic stroke. This strategy allows the detection and quantification of cerebral and carotid thrombi, and the ability to monitor tissue plasminogen activator therapy by CT imaging.⁶⁹

In cardiac imaging, CT offers superior evaluation of coronary lesion but lacks the capability to measure the transmural extent of scar tissue.^{129,130} In order to improve the detection sensitivity of scar tissue, Danila et al.⁷⁰ developed an innovative approach based on specific targeting of myocardial scar tissue. They coated GNPs (40–70 nm) with collagen targeting peptide (CNA35), a peptide against collagen-I, and injected them into mice with heart ischemia followed by reperfusion for 30 days (Figure 8, right panel). The images obtained using CT X-ray showed large scar tissue with focal contrast enhancement in the myocardium of mice subjected to heart ischemia. These results were further validated on histological staining. This was the first article to demonstrate the potential of CT to detect myocardial scar tissue by using GNPs coated with a collagen-homing peptide

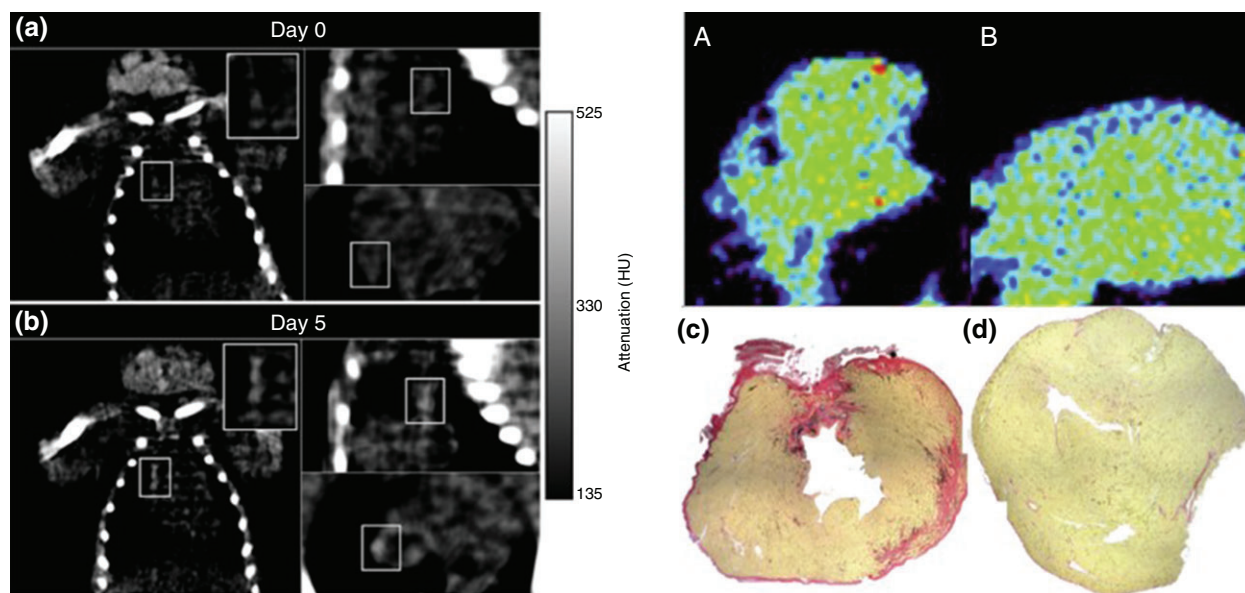


FIGURE 8 | Two examples of *in vivo* X-ray computed tomography (CT) imaging application in cardiovascular field using gold nanoparticles (GNPs) as contrast enhancement agents. Left panel: CT scans of an atherosclerotic mouse injected with gold-labeled monocytes on day 0 and day 5. White boxes indicate aortic region of interest. Attenuation increases in the aorta over 5 days as compared with the day 0. (Reprinted with permission from Ref 67. Copyright 2016 Elsevier). Right panel: CT imaging obtained in mice 30 days after ischemia–reperfusion of the heart. A hyperintense region (a) was detected by CT scanning in the myocardial scar corresponding to accumulation of GNPs targeting collagen-1 (CNA35-GNPs); no contrast enhancement was observed in control mice (b). On the histological slide stained with picosirius red (pink), the myocardial scar showed GNP retention after silver staining (black), with no GNPs presence in the control mouse (d). (Reprinted with permission from Ref 70. Copyright 2016 Elsevier)

on preclinical models. As the fibrous cap in atherosclerotic plaque is composed mainly of collagen and elastin, this strategy could be used to identify atherosclerotic plaques and thus to determine the plaque stability.

DISCUSSION AND FUTURE PERSPECTIVES

In this study, we described the preclinical applications of GNPs as contrast agents for optical and X-ray imaging in CVDs. The characteristics of GNPs (e.g., good chemical stability and *in vivo* biocompatibility) render them suitable as an exogenous contrast agent. Moreover, the optical properties of GNPs can be relatively easily tuned by changing the shape and size.

Different investigators have shown that GNPs with a size between 10 and 60 nm tend to accumulate into the atherosclerotic plaque by a passive mechanism such as macrophage uptake or by the enhanced permeability and retention (EPR) effect.¹³¹ However, at this size, they cannot be excreted by the kidneys and accumulate over the time into the spleen and liver.^{132,133}

Another manner to enhance the accumulation into a specific area is the targeting with antibodies, peptides, or HDLs. This renders GNPs interesting for noninvasive X-rays imaging, because iodine contrast agents are limited as they cannot be conjugated with biological markers for specific target localization. Moreover, compared with iodinated-contrast agents, GNPs possess a long circulation time. Different biomarkers are identified in CVDs. For example, plaque neoangiogenesis can induce rapid plaque growth by intraplaque hemorrhages, which lead to plaque rupture. A potential marker to detect neoangiogenesis is Integrin $\alpha_v\beta_3$, a cell surface glycoprotein receptor, expressed on activated endothelial cells and frequently used to visualize angiogenesis. Inflammation is another key feature of high-risk plaques and thus imaging of monocyte/macrophage accumulation into plaque can help to improve the patient's risk stratification. These markers allow the molecular imaging of atherosclerotic plaques or thrombosis and may improve the assessment of risk for acute complications.

The capacity of GNPs to accumulate at atherosclerotic plaque level, either directly by targeting endothelial cells or indirectly after their uptake by macrophages and subsequent accumulation into atherosclerotic plaque, raises another problem. This is linked to the fact that the massive accumulation of

GNPs could induce undesirable effects on the site of interest. Even if GNPs at therapeutic doses are not toxic when injected intravenously¹³⁴, *in vivo* toxicity has not been systematically evaluated in preclinical studies focused on applications of GNPs as contrast agents. It is known that the toxicity may be linked to the local concentration of GNPs. A better knowledge of the long-term fate of GNPs and their effects on targeted sites (e.g., atherosclerotic plaque, clot, and ischemic myocardium) of GNPs at long term is essential in the future.

Research in cardiovascular imaging continues to explore new frontiers. If the standard imaging modalities provide anatomical information, GNPs could be an added value for a personalized diagnosis. Despite encouraging preclinical results, the use of GNPs as contrast agent in cardiovascular field is still in its infancy. At present, no imaging modality meets clinical needs optimally. Developing multimodal imaging with GNPs would enable a wide range of anatomic, functional, and molecular information to better identify the high-risk lesions and subsequently prevention of future cardiovascular events. We note that the multimodal imaging strategies by using the same contrast agent permit to reduce repeated injection of the contrast agent, a better contrast enhancement of the targeted area and complementary information on the disease.

GNPs are able to create a signal enhancement either in photoacoustic or in OCT imaging. We note however a principal limitation linked to light penetration into deep tissues: while in a mouse model is relatively easy to detect an atherosclerotic plaque, in humans this become more complicated because of the deeper localization of the lesion (e.g., atherosclerotic plaque, clot, and ischemic myocardium). This can be partially overtaken by using an intravascular probe.

Further investigations and improvements of GNPs as contrast agents are needed before their clinical application. This involves a deeper evaluation of: the GNPs (size, local concentration, targeted, or not) the preclinical model and the type of imaging modality. For a potential cardiovascular clinical imaging translation, the size of GNPs should allow them to be gradually excreted by the kidney, and in the same time to have a large imaging window (and thus avoid repeated injection). Recently, Cheheltani et al.⁵⁰ synthesized such types of GNPs with potential applications in photoacoustic and CT imaging. Evaluation of the contrast enhancement on large preclinical models (e.g., pig) is essential before the translation to the clinics. For clinical applications, the choice of imaging technique (invasive vs noninvasive) using GNPs as contrast agents should

take into consideration the localization of the diseases, the resolution, and the sensitivity needed for a

better diagnostic, and thus an improved patient risk stratification.

ACKNOWLEDGMENTS

The authors acknowledge the support of the AXA Research Fund and the French National Research Agency (ANR-10-LABX-24 and ANR-10-IDEX-0001-02 PSL). They also thank M. Hill, A-M. Rosu, K. Flanagan, and F. Dormont for reviewing English usage and structure.

REFERENCES

1. Boisselier E, Astruc D. Gold nanoparticles in nanomedicine: preparations, imaging, diagnostics, therapies and toxicity. *Chem Soc Rev* 2009, 38:1759–1782.
2. Herizchi R, Abbasi E, Milani M, Akbarzadeh A. Current methods for synthesis of gold nanoparticles. *Artif Cells Nanomed Biotechnol* 2016, 44:596–602.
3. Willets KA, Van Duyne RP. Localized surface plasmon resonance spectroscopy and sensing. *Annu Rev Phys Chem* 2007, 58:267–297.
4. Thakor AS, Jokerst J, Zavaleta C, Massoud TF, Gambhir SS. Gold nanoparticles: a revival in precious metal administration to patients. *Nano Lett* 2011, 11:4029–4036.
5. Moyano DF, Duncan B, Rotello VM. Preparation of 2 nm gold nanoparticles for in vitro and in vivo applications. *Methods Mol Biol* 2013, 1025:3–8.
6. Chung TH, Wu SH, Yao M, Lu CW, Lin YS, Hung Y, Mou CY, Chen YC, Huang DM. The effect of surface charge on the uptake and biological function of mesoporous silica nanoparticles in 3 T3-L1 cells and human mesenchymal stem cells. *Biomaterials* 2007, 28:2959–2966.
7. Spivak MY, Bubnov RV, Yemets IM, Lazarenko LM, Tymoshok NO, Ulberg ZR. Gold nanoparticles—the theranostic challenge for PPPM: nanocardiology application. *EPMA J* 2013, 4:18.
8. Niidome T, Nakashima K, Takahashi H, Niidome Y. Preparation of primary amine-modified gold nanoparticles and their transfection ability into cultivated cells. *Chem Commun (Camb)* 2004:1978–1979.
9. Kumar D, Saini N, Jain N, Sareen R, Pandit V. Gold nanoparticles: an era in bionanotechnology. *Expert Opin Drug Deliv* 2013, 10:397–409.
10. Moghimi SM, Hunter AC, Murray JC. Nanomedicine: current status and future prospects. *FASEB J* 2005, 19:311–330.
11. Teranishi T, Eguchi M, Kanehara M, Gwo S. Controlled localized surface plasmon resonance wavelength for conductive nanoparticles over the ultraviolet to near-infrared region. *J Mater Chem* 2011, 21:10238–10242.
12. Huang X, Jain PK, El-Sayed IH, El-Sayed MA. Determination of the minimum temperature required for selective photothermal destruction of cancer cells with the use of immunotargeted gold nanoparticles. *Photochem Photobiol* 2006, 82:412–417.
13. Pan D, Pramanik M, Wickline SA, Wang LV, Lanza GM. Recent advances in colloidal gold nanobeacons for molecular photoacoustic imaging. *Contrast Media Mol Imaging* 2011, 6:378–388.
14. De La Vega JC, Hafeli UO. Utilization of nanoparticles as X-ray contrast agents for diagnostic imaging applications. *Contrast Media Mol Imaging* 2015, 10:81–95.
15. Massoud TF, Gambhir SS. Molecular imaging in living subjects: seeing fundamental biological processes in a new light. *Genes Dev* 2003, 17:545–580.
16. Murray CJL, Vos T, Lozano R, AlMazroa MA, Memish ZA. Disability-adjusted life years (DALYs) for 291 diseases and injuries in 21 regions, 1990–2010: a systematic analysis for the Global Burden of Disease Study 2010 (vol 380, pg 2197, 2012). *Lancet* 2013, 381:628.
17. Go AS, Mozaffarian D, Roger VL, Benjamin EJ, Berry JD, Borden WB, Bravata DM, Dai S, Ford ES, Fox CS, et al. Heart disease and stroke statistics-2013 update: a report from the American Heart Association. *Circulation* 2013, 127:e6–e245.
18. Moore KJ, Tabas I. Macrophages in the pathogenesis of atherosclerosis. *Cell* 2011, 145:341–355.
19. Quillard T, Libby P. Molecular imaging of atherosclerosis for improving diagnostic and therapeutic development. *Circ Res* 2012, 111:231–244.
20. Silvestre-Roig C, de Winther MP, Weber C, Daemen MJ, Lutgens E, Soehnlein O. Atherosclerotic plaque destabilization: mechanisms, models, and therapeutic strategies. *Circ Res* 2014, 114:214–226.
21. Bentzon JF, Otsuka F, Virmani R, Falk E. Mechanisms of plaque formation and rupture. *Circ Res* 2014, 114:1852–1866.
22. Weber C, Noels H. Atherosclerosis: current pathogenesis and therapeutic options. *Nat Med* 2011, 17:1410–1422.

23. Skeoch S, Bruce IN. Atherosclerosis in rheumatoid arthritis: is it all about inflammation? *Nat Rev Rheumatol* 2015, 11:390–400.
24. Maiolino G, Rossitto G, Caielli P, Bisogni V, Rossi GP, Calo LA. The role of oxidized low-density lipoproteins in atherosclerosis: the myths and the facts. *Mediators Inflamm* 2013, 2013:714653.
25. Glass CK, Witztum JL. Atherosclerosis. the road ahead. *Cell* 2001, 104:503–516.
26. Varna M, Juenet M, Bayles R, Mazighi M, Chauvierre C, Letourneur D. Nanomedicine as a strategy to fight thrombotic diseases. *Future Sci OA* 2015, 1:1–14.
27. Hilgendorf I, Swirski FK, Robbins CS. Monocyte fate in atherosclerosis. *Arterioscler Thromb Vasc Biol* 2015, 35:272–279.
28. Falk E. Pathogenesis of atherosclerosis. *J Am Coll Cardiol* 2006, 47:C7–C12.
29. Furie B, Furie BC. Mechanisms of thrombus formation. *N Engl J Med* 2008, 359:938–949.
30. Erbel R, Aboyans V, Boileau C, Bossone E, Bartolomeo RD, Eggebrecht H, Evangelista A, Falk V, Frank H, Gaemperli O, et al. 2014 ESC Guidelines on the diagnosis and treatment of aortic diseases: document covering acute and chronic aortic diseases of the thoracic and abdominal aorta of the adult. The Task Force for the Diagnosis and Treatment of Aortic Diseases of the European Society of Cardiology (ESC). *Eur Heart J* 2014, 35:2873–2926.
31. Mathers CD, Loncar D. Projections of global mortality and burden of disease from 2002 to 2030. *PLoS Med* 2006, 3:e442.
32. Vancaeynest D, Pasquet A, Roelants V, Gerber BL, Vanoverschelde JL. Imaging the vulnerable plaque. *J Am Coll Cardiol* 2011, 57:1961–1979.
33. Cai J, Hatsukami TS, Ferguson MS, Kerwin WS, Saam T, Chu B, Takaya N, Polissar NL, Yuan C. In vivo quantitative measurement of intact fibrous cap and lipid-rich necrotic core size in atherosclerotic carotid plaque: comparison of high-resolution, contrast-enhanced magnetic resonance imaging and histology. *Circulation* 2005, 112:3437–3444.
34. Kampschulte A, Ferguson MS, Kerwin WS, Polissar NL, Chu B, Saam T, Hatsukami TS, Yuan C. Differentiation of intraplaque versus juxtalumenal hemorrhage/thrombus in advanced human carotid atherosclerotic lesions by in vivo magnetic resonance imaging. *Circulation* 2004, 110:3239–3244.
35. Fayad ZA, Fuster V, Fallon JT, Jayasundera T, Worthley SG, Helft G, Aguinaldo JG, Badimon JJ, Sharma SK. Noninvasive in vivo human coronary artery lumen and wall imaging using black-blood magnetic resonance imaging. *Circulation* 2000, 102:506–510.
36. Fayad ZA, Nahar T, Fallon JT, Goldman M, Aguinaldo JG, Badimon JJ, Shinnar M, Chesebro JH, Fuster V. In vivo magnetic resonance evaluation of atherosclerotic plaques in the human thoracic aorta: a comparison with transesophageal echocardiography. *Circulation* 2000, 101:2503–2509.
37. Juenet M, Varna M, Aid-Launais R, Chauvierre C, Letourneur D. Nanomedicine for the molecular diagnosis of cardiovascular pathologies. *Biochem Biophys Res Commun* 2015, 468:476–484.
38. Di Carli MF, Dorbala S. Cardiac PET-CT. *J Thorac Imaging* 2007, 22:101–106.
39. Celebi AS, Yalcin H, Yalcin F. Current cardiac imaging techniques for detection of left ventricular mass. *Cardiovasc Ultrasound* 2010, 8:19.
40. Miller TD, Askew JW, Anavekar NS. Noninvasive stress testing for coronary artery disease. *Cardiol Clin* 2014, 32:387–404.
41. Swallow RA, Court IA, Calver AL, Curzen NP. The limitations of coronary angiography: identification of a critical coronary stenosis using intravascular ultrasound. *Int J Cardiol* 2006, 106:123–125.
42. Nissen SE, Yock P. Intravascular ultrasound: novel pathophysiological insights and current clinical applications. *Circulation* 2001, 103:604–616.
43. Fujimoto JG, Pitris C, Boppart SA, Brezinski ME. Optical coherence tomography: an emerging technology for biomedical imaging and optical biopsy. *Neoplasia* 2000, 2:9–25.
44. Wang TY, Mancuso JJ, Kazmi SMS, Dwelle J, Sapozhnikova V, Willsey B, Ma LL, Qiu JZ, Li XK, Dunn AK, et al. Combined two-photon luminescence microscopy and OCT for macrophage detection in the hypercholesterolemic rabbit aorta using plasmonic gold nanorose. *Lasers Surg Med* 2012, 44:49–59.
45. Tearney GJ, Regar E, Akasaka T, Adriaenssens T, Barlis P, Bezerra HG, Bouma B, Bruining N, Cho JM, Chowdhary S, et al. Consensus standards for acquisition, measurement, and reporting of intravascular optical coherence tomography studies: a report from the International Working Group for Intravascular Optical Coherence Tomography Standardization and Validation. *J Am Coll Cardiol* 2012, 59:1058–1072.
46. Sinclair H, Bourantas C, Bagnall A, Mintz GS, Kunadian V. OCT for the identification of vulnerable plaque in acute coronary syndrome. *JACC Cardiovasc Imaging* 2015, 8:198–209.
47. Song KH, Wang LV. Noninvasive photoacoustic imaging of the thoracic cavity and the kidney in small and large animals. *Med Phys* 2008, 35:4524–4529.
48. Li W, Brown PK, Wang LV, Xia Y. Gold nanocages as contrast agents for photoacoustic imaging. *Contrast Media Mol Imaging* 2011, 6:370–377.
49. Lemaster JE, Jokerst JV. What is new in nanoparticle-based photoacoustic imaging? *Wiley Interdiscip Rev*

- Nanomed Nanobiotechnol* 2017, 9:e1404. doi:10.1002/wnan.1404.
50. Cheheltani R, Ezzibdeh RM, Chhour P, Pulaparthi K, Kim J, Jurcova M, Hsu JC, Blundell C, Litt HI, Ferrari VA, et al. Tunable, biodegradable gold nanoparticles as contrast agents for computed tomography and photoacoustic imaging. *Biomaterials* 2016, 102:87–97.
 51. Pan D, Pramanik M, Senpan A, Allen JS, Zhang H, Wickline SA, Wang LV, Lanza GM. Molecular photoacoustic imaging of angiogenesis with integrin-targeted gold nanobecons. *FASEB J* 2011, 25:875–882.
 52. Alander JT, Kaartinen I, Laakso A, Patila T, Spillmann T, Tuchin VV, Venermo M, Valisuo P. A review of indocyanine green fluorescent imaging in surgery. *Int J Biomed Imaging* 2012, 2012:940585.
 53. Zhong J, Yang S, Zheng X, Zhou T, Xing D. In vivo photoacoustic therapy with cancer-targeted indocyanine green-containing nanoparticles. *Nanomedicine (Lond)* 2013, 8:903–919.
 54. Ueda S, Kuji I, Shigekawa T, Takeuchi H, Sano H, Hirokawa E, Shimada H, Suzuki H, Oda M, Osaki A, et al. Optical imaging for monitoring tumor oxygenation response after initiation of single-agent bevacizumab followed by cytotoxic chemotherapy in breast cancer patients. *PLoS One* 2014, 9:e98715.
 55. Douma K, Megens RT, van Zandvoort MA. Optical molecular imaging of atherosclerosis using nanoparticles: shedding new light on the darkness. *Wiley Interdiscip Rev Nanomed Nanobiotechnol* 2011, 3:376–388.
 56. Yao J, Maslov K, Hu S, Wang LV. Evans blue dye-enhanced capillary-resolution photoacoustic microscopy in vivo. *J Biomed Opt* 2009, 14:054049.
 57. Morgounova E, Shao Q, Hackel BJ, Thomas DD, Ashkenazi S. Photoacoustic lifetime contrast between methylene blue monomers and self-quenched dimers as a model for dual-labeled activatable probes. *J Biomed Opt* 2013, 18:56004.
 58. Weber J, Beard PC, Bohndiek SE. Contrast agents for molecular photoacoustic imaging. *Nat Methods* 2016, 13:639–650.
 59. Lu W, Huang Q, Ku G, Wen X, Zhou M, Guzatov D, Brecht P, Su R, Oraevsky A, Wang LV, et al. Photoacoustic imaging of living mouse brain vasculature using hollow gold nanospheres. *Biomaterials* 2010, 31:2617–2626.
 60. Rouleau L, Berti R, Ng VW, Matteau-Pelletier C, Lam T, Saboural P, Kakkar AK, Lesage F, Rheume E, Tardif JC. VCAM-1-targeting gold nanoshell probe for photoacoustic imaging of atherosclerotic plaque in mice. *Contrast Media Mol Imaging* 2013, 8:27–39.
 61. Pan D, Pramanik M, Senpan A, Yang X, Song KH, Scott MJ, Zhang H, Gaffney PJ, Wickline SA, Wang LV, et al. Molecular photoacoustic tomography with colloidal nanobecons. *Angew Chem Int Ed Engl* 2009, 48:4170–4173.
 62. Wang B, Yantsen E, Larson T, Karpouk AB, Sethuraman S, Su JL, Sokolov K, Emelianov SY. Plasmonic intravascular photoacoustic imaging for detection of macrophages in atherosclerotic plaques. *Nano Lett* 2009, 9:2212–2217.
 63. Yeager D, Karpouk A, Wang B, Amirian J, Sokolov K, Smalling R, Emelianov S. Intravascular photoacoustic imaging of exogenously labeled atherosclerotic plaque through luminal blood. *J Biomed Opt* 2012, 17:106016.
 64. Paranjape AS, Kuranov R, Baranov S, Ma LL, Villard JW, Wang TY, Sokolov KV, Feldman MD, Johnston KP, Milner TE. Depth resolved photothermal OCT detection of macrophages in tissue using nanorose. *Biomed Opt Express* 2010, 1:2–16.
 65. McQueenie R, Stevenson R, Benson R, MacRitchie N, McInnes I, Maffia P, Faulds K, Graham D, Brewer J, Garside P. Detection of inflammation in vivo by surface-enhanced Raman scattering provides higher sensitivity than conventional fluorescence imaging. *Anal Chem* 2012, 84:5968–5975.
 66. Cormode DP, Roessl E, Thran A, Skajaa T, Gordon RE, Schlomka JP, Fuster V, Fisher EA, Mulder WJ, Proksa R, et al. Atherosclerotic plaque composition: analysis with multicolor CT and targeted gold nanoparticles. *Radiology* 2010, 256:774–782.
 67. Chhour P, Naha PC, O'Neill SM, Litt HI, Reilly MP, Ferrari VA, Cormode DP. Labeling monocytes with gold nanoparticles to track their recruitment in atherosclerosis with computed tomography. *Biomaterials* 2016, 87:93–103.
 68. Kim DE, Kim JY, Sun IC, Schellingerhout D, Lee SK, Ahn CH, Kwon IC, Kim K. Hyperacute direct thrombus imaging using computed tomography and gold nanoparticles. *Ann Neurol* 2013, 73:617–625.
 69. Kim JY, Ryu JH, Schellingerhout D, Sun IC, Lee SK, Jeon S, Kim J, Kwon IC, Nahrendorf M, Ahn CH, et al. Direct imaging of cerebral thromboemboli using computed tomography and fibrin-targeted gold nanoparticles. *Theranostics* 2015, 5:1098–1114.
 70. Danila D, Johnson E, Kee P. CT imaging of myocardial scars with collagen-targeting gold nanoparticles. *Nanomedicine* 2013, 9:1067–1076.
 71. Wang YW, Xie XY, Wang XD, Ku G, Gill KL, O'Neal DP, Stoica G, Wang LV. Photoacoustic tomography of a nanoshell contrast agent in the in vivo rat brain. *Nano Lett* 2004, 4:1689–1692.
 72. Yang X, Skrabalak SE, Li ZY, Xia Y, Wang LV. Photoacoustic tomography of a rat cerebral cortex in vivo with Au nanocages as an optical contrast agent. *Nano Lett* 2007, 7:3798–3802.

73. Kim K, Huang SW, Ashkenazi S, O'Donnell M, Agarwal A, Kotov NA, Denny MF, Kaplan MJ. Photoacoustic imaging of early inflammatory response using gold nanorods. *Appl Phys Lett* 2007, 90. doi:10.1063/1.2743752.
74. Li PC, Wang CR, Shieh DB, Wei CW, Liao CK, Poe C, Jhan S, Ding AA, Wu YN. In vivo photoacoustic molecular imaging with simultaneous multiple selective targeting using antibody-conjugated gold nanorods. *Opt Express* 2008, 16:18605–18615.
75. Iiyama K, Hajra L, Iiyama M, Li H, DiChiara M, Medoff BD, Cybulsky MI. Patterns of vascular cell adhesion molecule-1 and intercellular adhesion molecule-1 expression in rabbit and mouse atherosclerotic lesions and at sites predisposed to lesion formation. *Circ Res* 1999, 85:199–207.
76. Wang PH, Liu HL, Hsu PH, Lin CY, Wang CR, Chen PY, Wei KC, Yen TC, Li ML. Gold-nanorod contrast-enhanced photoacoustic micro-imaging of focused-ultrasound induced blood–brain-barrier opening in a rat model. *J Biomed Opt* 2012, 17:061222.
77. Ricles LM, Nam SY, Sokolov K, Emelianov SY, Suggs LJ. Function of mesenchymal stem cells following loading of gold nanotracers. *Int J Nanomedicine* 2011, 6:407–416.
78. Joshi PP, Yoon SJ, Chen YS, Emelianov S, Sokolov KV. Development and optimization of near-IR contrast agents for immune cell tracking. *Biomed Opt Express* 2013, 4:2609–2618.
79. Wang B, Su JL, Amirian J, Litovsky SH, Smalling R, Emelianov S. Detection of lipid in atherosclerotic vessels using ultrasound-guided spectroscopic intravascular photoacoustic imaging. *Opt Express* 2010, 18:4889–4897.
80. Batty JA, Subba S, Luke P, Gigi LW, Sinclair H, Kunadian V. Intracoronary imaging in the detection of vulnerable plaques. *Curr Cardiol Rep* 2016, 18:28.
81. Jansen K, van Soest G, van der Steen AF. Intravascular photoacoustic imaging: a new tool for vulnerable plaque identification. *Ultrasound Med Biol* 2014, 40:1037–1048.
82. Razansky D, Baeten J, Ntziachristos V. Sensitivity of molecular target detection by multispectral optoacoustic tomography (MSOT). *Med Phys* 2009, 36:939–945.
83. Taruttis A, Wildgruber M, Kosanke K, Beziere N, Licha K, Haag R, Aichler M, Walch A, Rummeny E, Ntziachristos V. Multispectral optoacoustic tomography of myocardial infarction. *Photoacoustics* 2013, 1:3–8.
84. McNally LR, Mezera M, Morgan DE, Frederick PJ, Yang ES, Eltoun IE, Grizzle WE. Current and emerging clinical applications of multispectral optoacoustic tomography (MSOT) in oncology. *Clin Cancer Res* 2016, 22:3432–3439.
85. Taruttis A, Herzog E, Razansky D, Ntziachristos V. Real-time imaging of cardiovascular dynamics and circulating gold nanorods with multispectral optoacoustic tomography. *Opt Express* 2010, 18:19592–19602.
86. Taruttis A, Claussen J, Razansky D, Ntziachristos V. Motion clustering for deblurring multispectral optoacoustic tomography images of the mouse heart. *J Biomed Opt* 2012, 17:016009.
87. Nahas A, Varna M, Fort E, Boccara AC. Detection of plasmonic nanoparticles with full field-OCT: optical and photothermal detection. *Biomed Opt Express* 2014, 5:3541–3546.
88. Cauberg EC, de Bruin DM, Faber DJ, van Leeuwen TG, de la Rosette JJ, de Reijke TM. A new generation of optical diagnostics for bladder cancer: technology, diagnostic accuracy, and future applications. *Eur Urol* 2009, 56:287–296.
89. Coletta J, Suzuki N, Nascimento BR, Bezerra HG, Rosenthal N, Guagliumi G, Rollins AM, Costa MA. Use of optical coherence tomography for accurate characterization of atherosclerosis. *Arq Bras Cardiol* 2010, 94:250–254, 268–272, 254–259.
90. Tearney GJ, Jang IK, Bouma BE. Optical coherence tomography for imaging the vulnerable plaque. *J Biomed Opt* 2006, 11:021002.
91. Zysk AM, Nguyen FT, Oldenburg AL, Marks DL, Boppart SA. Optical coherence tomography: a review of clinical development from bench to bedside. *J Biomed Opt* 2007, 12:051403.
92. Villard JW, Paranjape AS, Victor DA, Feldman MD. Applications of optical coherence tomography in cardiovascular medicine, part 2. *J Nucl Cardiol* 2009, 16:620–639.
93. Yamaguchi T, Terashima M, Akasaka T, Hayashi T, Mizuno K, Muramatsu T, Nakamura M, Nakamura S, Saito S, Takano M, et al. Safety and feasibility of an intravascular optical coherence tomography image wire system in the clinical setting. *Am J Cardiol* 2008, 101:562–567.
94. Kubo T, Tanaka A, Kitabata H, Ino Y, Tanimoto T, Akasaka T. Application of optical coherence tomography in percutaneous coronary intervention. *Circ J* 2012, 76:2076–2083.
95. Kubo T, Tanaka A, Ino Y, Kitabata H, Shiono Y, Akasaka T. Assessment of coronary atherosclerosis using optical coherence tomography. *J Atheroscler Thromb* 2014, 21:895–903.
96. Jung Y, Guan G, Wei CW, Reif R, Gao X, O'Donnell M, Wang RK. Multifunctional nanoprobe to enhance the utility of optical based imaging techniques. *J Biomed Opt* 2012, 17:016015.
97. Eghtedari M, Oraevsky A, Copland JA, Kotov NA, Conjusteau A, Motamedi M. High sensitivity of in vivo detection of gold nanorods using a laser

- optoacoustic imaging system. *Nano Lett* 2007, 7:1914–1918.
98. Song KH, Kim C, Maslov K, Wang LV. Noninvasive in vivo spectroscopic nanorod-contrast photoacoustic mapping of sentinel lymph nodes. *Eur J Radiol* 2009, 70:227–231.
99. Webb JA, Bardhan R. Emerging advances in nanomedicine with engineered gold nanostructures. *Nano-scale* 2014, 6:2502–2530.
100. Agrawal A, Huang S, Wei Haw Lin A, Lee MH, Barton JK, Drezek RA, Pfefer TJ. Quantitative evaluation of optical coherence tomography signal enhancement with gold nanoshells. *J Biomed Opt* 2006, 11:041121.
101. Gobin AM, Lee MH, Halas NJ, James WD, Drezek RA, West JL. Near-infrared resonant nanoshells for combined optical imaging and photothermal cancer therapy. *Nano Lett* 2007, 7:1929–1934.
102. Zagaynova EV, Shirmanova MV, Kirillin MY, Khlebtsov BN, Orlova AG, Balalaeva IV, Sirotkina MA, Bugrova ML, Agrba PD, Kamensky VA. Contrasting properties of gold nanoparticles for optical coherence tomography: phantom, in vivo studies and Monte Carlo simulation. *Phys Med Biol* 2008, 53:4995–5009.
103. Boyer D, Tamarat P, Maali A, Lounis B, Orrit M. Photothermal imaging of nanometer-sized metal particles among scatterers. *Science* 2002, 297:1160–1163.
104. Kim J, Oh J, Milner TE. Measurement of optical path length change following pulsed laser irradiation using differential phase optical coherence tomography. *J Biomed Opt* 2006, 11. doi:10.1117/1.2236289.
105. Tucker-Schwartz JM, Meyer TA, Patil CA, Duvall CL, Skala MC. In vivo photothermal optical coherence tomography of gold nanorod contrast agents. *Biomed Opt Express* 2012, 3:2881–2895.
106. Hu J, Rivero F, Torres RA, Loro Ramirez H, Rodriguez EM, Alfonso F, Garcia Sole J, Jaque D. Dynamic single gold nanoparticle visualization by clinical intracoronary optical coherence tomography. *J Biophotonics* 2016. doi:10.1002/jbio.201600062.
107. Hanlon EB, Manoharan R, Koo TW, Shafer KE, Motz JT, Fitzmaurice M, Kramer JR, Itzkan I, Dasari RR, Feld MS. Prospects for in vivo Raman spectroscopy. *Phys Med Biol* 2000, 45:R1–R59.
108. Schlucker S. SERS microscopy: nanoparticle probes and biomedical applications. *Chemphyschem* 2009, 10:1344–1354.
109. Zhang Y, Hong H, Cai W. Imaging with Raman spectroscopy. *Curr Pharm Biotechnol* 2010, 11:654–661.
110. Yuan H, Liu Y, Fales AM, Li YL, Liu J, Vo-Dinh T. Quantitative surface-enhanced resonant Raman scattering multiplexing of biocompatible gold nanostars for in vitro and ex vivo detection. *Anal Chem* 2013, 85:208–212.
111. Jung S, Nam J, Hwang S, Park J, Hur J, Im K, Park N, Kim S. Theragnostic pH-sensitive gold nanoparticles for the selective surface enhanced Raman scattering and photothermal cancer therapy. *Anal Chem* 2013, 85:7674–7681.
112. Hu J, Zhu X, Li H, Zhao Z, Chi X, Huang G, Huang D, Liu G, Wang X, Gao J. Theranostic Au cubic nano-aggregates as potential photoacoustic contrast and photothermal therapeutic agents. *Theranostics* 2014, 4:534–545.
113. Qian X, Peng XH, Ansari DO, Yin-Goen Q, Chen GZ, Shin DM, Yang L, Young AN, Wang MD, Nie S. In vivo tumor targeting and spectroscopic detection with surface-enhanced Raman nanoparticle tags. *Nat Biotechnol* 2008, 26:83–90.
114. Conde J, Bao C, Cui D, Baptista PV, Tian F. Antibody-drug gold nanoantennas with Raman spectroscopic fingerprints for in vivo tumour theranostics. *J Control Release* 2014, 183:87–93.
115. Li T, Guo L, Wang Z. Gold nanoparticle-based surface enhanced Raman scattering spectroscopic assay for the detection of protein-protein interactions. *Anal Sci* 2008, 24:907–910.
116. Banholzer MJ, Millstone JE, Qin L, Mirkin CA. Rationally designed nanostructures for surface-enhanced Raman spectroscopy. *Chem Soc Rev* 2008, 37:885–897.
117. Culha M, Cullum B, Lavrik N, Klutse CK. Surface-enhanced Raman scattering as an emerging characterization and detection technique. *J Nanotechnol* 2012, 2012:15.
118. Samanta A, Maiti KK, Soh KS, Liao X, Vendrell M, Dinish US, Yun SW, Bhuvaneshwari R, Kim H, Rautela S, et al. Ultrasensitive near-infrared Raman reporters for SERS-based in vivo cancer detection. *Angew Chem Int Ed Engl* 2011, 50:6089–6092.
119. Silva WR, Keller EL, Frontiera RR. Determination of resonance Raman cross-sections for use in biological SERS sensing with femtosecond stimulated Raman spectroscopy. *Anal Chem* 2014, 86:7782–7787.
120. Yu SB, Watson AD. Metal-based X-ray contrast media. *Chem Rev* 1999, 99:2353–2378.
121. Liu Y, Ai K, Lu L. Nanoparticulate X-ray computed tomography contrast agents: from design validation to in vivo applications. *Acc Chem Res* 2012, 45:1817–1827.
122. Cole L, Vargo-Gogola T, Roeder R. Gold nanoparticles enable improved sensitivity and specificity for X-ray detection of microcalcifications in radiographically dense mammary tissues. *J Nucl Med* 2015, 56:4–5.
123. Cole LE, Ross RD, Tilley JMR, Vargo-Gogola T, Roeder RK. Gold nanoparticles as contrast agents in

- X-ray imaging and computed tomography. *Nanomedicine* 2015, 10:321–341.
124. Stacul F, van der Molen AJ, Reimer P, Webb JA, Thomsen HS, Morcos SK, Almen T, Aspelin P, Bellin MF, Clement O, et al. Contrast induced nephropathy: updated ESUR Contrast Media Safety Committee guidelines. *Eur Radiol* 2011, 21:2527–2541.
 125. Hainfeld JF, Slatkin DN, Smilowitz HM. The use of gold nanoparticles to enhance radiotherapy in mice. *Phys Med Biol* 2004, 49:N309–N315.
 126. Hainfeld JF, Slatkin DN, Focella TM, Smilowitz HM. Gold nanoparticles: a new X-ray contrast agent. *Br J Radiol* 2006, 79:248–253.
 127. Alivov Y, Baturin P, Le HQ, Ducote J, Molloy S. Optimization of K-edge imaging for vulnerable plaques using gold nanoparticles and energy resolved photon counting detectors: a simulation study. *Phys Med Biol* 2014, 59:135–152.
 128. Bulte JW. Science to practice: can CT be performed for multicolor molecular imaging? *Radiology* 2010, 256:675–676.
 129. Rodriguez-Granillo GA, Rosales MA, Degrossi E, Rodriguez AE. Signal density of left ventricular myocardial segments and impact of beam hardening artifact: implications for myocardial perfusion assessment by multidetector CT coronary angiography. *Int J Cardiovasc Imaging* 2010, 26:345–354.
 130. Crossett MP, Schneider-Kolsky M, Troupis J. Normal perfusion of the left ventricular myocardium using 320 MDCT. *J Cardiovasc Comput Tomogr* 2011, 5:406–411.
 131. Kim Y, Lobatto ME, Kawahara T, Lee Chung B, Mieszawska AJ, Sanchez-Gaytan BL, Fay F, Senders ML, Calcagno C, Becraft J, et al. Probing nanoparticle translocation across the permeable endothelium in experimental atherosclerosis. *Proc Natl Acad Sci USA* 2014, 111:1078–1083.
 132. Fitzpatrick JA, Andreko SK, Ernst LA, Waggoner AS, Ballou B, Bruchez MP. Long-term persistence and spectral blue shifting of quantum dots in vivo. *Nano Lett* 2009, 9:2736–2741.
 133. Sadauskas E, Danscher G, Stoltenberg M, Vogel U, Larsen A, Wallin H. Protracted elimination of gold nanoparticles from mouse liver. *Nanomedicine* 2009, 5:162–169.
 134. Pannerec-Varna M, Ratajczak P, Bousquet G, Ferreira I, Leboeuf C, Boisgard R, Gapihan G, Verine J, Palpant B, Bossy E, et al. In vivo uptake and cellular distribution of gold nanoshells in a preclinical model of xenografted human renal cancer. *Gold Bull* 2013, 46:257–265.